*J. Fluid Mech.* (2010), *vol.* 652, *pp.* 489–499.  
doi:10.1017/S0022112010000741

# Effective slip in pressure-driven flow past super-hydrophobic stripes

A. V. BELYAEV[1,2] AND O. I. VINOGRADOVA[1,2,3]†

[1]Departments of Physics and Chemistry, M. V. Lomonosov Moscow State University, 119991 Moscow, Russia

[2]A. N. Frumkin Institute of Physical Chemistry and Electrochemistry, Russian Academy of Sciences, 31 Leninsky Prospect, 119991 Moscow, Russia

[3]ITMC and DWI, RWTH Aachen, Pauwelsstrasse 8, 52056 Aachen, Germany

(Received 27 November 2009; revised 5 February 2010; accepted 5 February 2010)

A super-hydrophobic array of grooves containing trapped gas (stripes) has the potential to greatly reduce drag and enhance mixing phenomena in microfluidic devices. Recent work has focused on idealized cases of stick-perfect slip stripes. Here, we analyse the experimentally more relevant situation of a pressure-driven flow past striped slip-stick surfaces with arbitrary local slip at the gas sectors. We derive approximate formulas for maximal (longitudinal) and minimal (transverse) directional effective slip lengths that are in a good agreement with the exact numerical solution for any surface slip fraction. By representing eigenvalues of the slip length tensor, we obtain the effective slip for any orientation of stripes with respect to the mean flow. Our results imply that flow past stripes is controlled by the ratio of the local slip length to texture size. In the case of a large (compared to the texture period) slip at the gas areas, surface anisotropy leads to a tensorial effective slip, by attaining the values predicted earlier for a perfect local slip. Both effective slip lengths and anisotropy of the flow decrease when local slip becomes of the order of texture period. In the case of a small slip, we predict simple surface-averaged isotropic flows (independent of orientation).

## 1. Introduction

The development of microfluidics has motivated interest in manipulating flows in very small channels (Stone, Stroock & Ajdari 2004; Squires & Quake 2005). Most microfluidic devices operate with a pressure flow, which is faced with two main difficulties at this scale and under typical operating conditions. Firstly, it is difficult to drive such a flow due to huge hydrodynamic resistance. Secondly, it is very difficult to mix, which normally requires a generation of a transverse flow.

An efficient strategy for moving fluid in a tiny channel is to exploit hydrodynamic slip, which can be generated at hydrophobic surfaces and is quantified by the slip length $b$ (the distance within the solid at which the flow profile extrapolates to zero) (Vinogradova 1999; Bocquet & Barrat 2007; Lauga, Brenner & Stone 2007). Since for hydrophobic smooth and homogeneous surfaces the slip length can be of the order of tens of nanometres (Vinogradova & Yakubov 2003; Cottin-Bizonne *et al.* 2005; Joly, Ybert & Bocquet 2006; Vinogradova *et al.* 2009), but not much more, it

† Email address for correspondence: oivinograd@yahoo.com

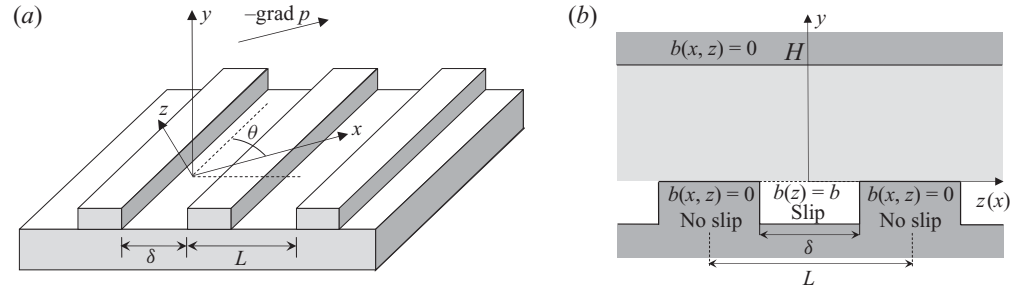


FIGURE 1. (*a*) Sketch of SH stripes: $\theta = \pi/2$ corresponds to transverse, whereas $\theta = 0$ to longitudinal stripes; (*b*) situation in (*a*) is approximated by a periodic cell of size $L$, with equivalent flow boundary conditions on gas–liquid and solid–liquid interface.

is impossible to benefit from such a nanometric slip for pressure-driven microfluidic applications. However, super-hydrophobic (SH) textures can significantly amplify hydrodynamic slip due to gas entrapment (Vinogradova *et al.* 1995; Cottin-Bizonne *et al.* 2003) leading to a huge slip length at the gas area. The composite nature of the texture, however, requires regions of lower slip (or no slip) in direct contact with the liquid, so the effective slip length of the surface $b_{eff}$ is reduced. Indeed, experimental studies of flow past SH surfaces suggest that effective slip is of the order of several microns (Ou & Rothstein 2005; Choi *et al.* 2006; Joseph *et al.* 2006).

SH surfaces consisting of a periodic array of grooves containing trapped gas (Cassie's state) are especially interesting since they allow us to highlight effects of anisotropy. For anisotropic textures $b_{eff}$ varies with the orientation of the wall texture relative to flow and is generally a tensor (Bazant & Vinogradova 2008). Such surfaces have been already used for reduction in pressure-driven flows (Ou & Rothstein 2005) and enhancement of mixing (Ou, Moss & Rothstein 2007). The problem of flow past stripes has been examined theoretically mostly with a typical geometry sketched in figure 1 corresponding to a roughly flat (no meniscus curvature) liquid interface, so that the modelled SH surface appeared as perfectly smooth with a pattern of boundary conditions. In the case of thin channels ($H \ll L$, where $H$ is the channel thickness, and $L$ is the period of the texture) the problem was solved for any two-component (e.g. low slip and high slip) texture, and striped surfaces were shown to provide rigorous upper and lower bounds on the effective slip over all possible two-phase patterns (Feuillebois, Bazant & Vinogradova 2009). The quantitative understanding of liquid slippage past such a surface in the thick channel ($H \gg L$) is however still challenging. Pressure-driven flow has been analysed for an idealized case of a perfect slip at the gas area (Philip 1972; Lauga & Stone 2003; Cottin-Bizonne *et al.* 2004; Sbragaglia & Prosperetti 2007) and led to

$$b_{eff}^{\perp} = \frac{L}{2\pi}\ln\left[\sec\left(\frac{\pi\phi_2}{2}\right)\right] \quad \text{and} \quad b_{eff}^{\parallel} = 2b_{eff}^{\perp}, \tag{1.1}$$

where $\phi_2 = \delta/L$ denotes the fraction of the liquid–gas interface (correspondingly, $\phi_1 = 1 - \phi_2$ is the fraction of solid–gas area), with the typical length scale of the slipping area $\delta$, and $b_{eff}^{\perp}$ and $b_{eff}^{\parallel}$ denote effective transverse and longitudinal slip lengths. Following Bazant & Vinogradova (2008), these are the eigenvalues of the second-rank effective slip-length tensor $\boldsymbol{b}_{eff}$ represented by a symmetric positive

definite $2 \times 2$ matrix diagonalized by a rotation:

$$\boldsymbol{b}_{eff} = \boldsymbol{S}_\theta \begin{pmatrix} b_{eff}^{\parallel} & 0 \\ 0 & b_{eff}^{\perp} \end{pmatrix} \boldsymbol{S}_{-\theta}, \quad \boldsymbol{S}_\theta = \begin{pmatrix} \cos\theta & \sin\theta \\ -\sin\theta & \cos\theta \end{pmatrix}. \tag{1.2}$$

Therefore, (1.1) allow us to calculate $b_{eff}$ in any direction given by an angle $\theta$ (figure 1).

Equations (1.1) provide an upper limit for the effective slip lengths and in many situations it would be expected to overestimate them. One reason is the possible meniscus curvature, which has been clarified in some recent works (Sbragaglia & Prosperetti 2007; Hyväluoma & Harting 2008; Davis & Lauga 2009) and another reason is viscous dissipation taking place in the underlying gas phase. Indeed, the more realistic 'gas cushion model' (Vinogradova 1995) predicts the finite slip length at the slipping area

$$b = e\left(\frac{\eta}{\eta_g} - 1\right) \approx e\frac{\eta}{\eta_g}, \tag{1.3}$$

where $e$ is the thickness of the gas layer, $\eta$ is the viscosity of liquid and $\eta_g$ is the viscosity of gas. Taking into account that under typical conditions $\eta/\eta_g \approx 50$, the variation of the SH texture height, $e$, in the typical interval 0.1–10 μm (Quere 2005) gives $b$ = 5–500 μm, i.e. $b$ might be as small as typical $L$ or even less. For this reason, it is attractive to consider this experimentally relevant situation. However, despite its fundamental and practical significance, pressure-driven flow over partial slip stripes has received little attention. This has been studied numerically (Cottin-Bizonne *et al.* 2004; Priezjev, Darhuber & Troian 2005; Ybert *et al.* 2007). Nevertheless, no analytical resolution of the Stokes equation with this set of boundary conditions has been performed up to now.

In this paper, we provide analytical solutions to pressure-driven flows over SH stripes. In § 2 we formulate the problem and derive expressions for the effective slip for longitudinal and transverse stripes, which allow us to obtain a solution for any orientation of stripes with respect to a gradient of pressure. In § 3 we compare our results with numerical calculations performed by C. Cottin-Bizonne and C. Barentin using the method developed in Cottin-Bizonne *et al.* (2004) and discuss implications for the use of SH stripes to control hydrodynamic flows. We conclude in § 4.

## 2. Model and analysis

We consider a pressure-driven flow past an idealized flat periodic striped SH surface in the Cassie state (sketched in figure 1), where the liquid–solid interface has no slip ($b_1 = 0$) and the liquid–gas interface has partial slip ($b_2 = b$). Our results apply to a single surface in a thick channel ($H \gg \max\{L, b\}$), but not to thin channels ($H \ll \min\{L, b\}$) where the effective slip scales with the channel width (Feuillebois *et al.* 2009). The origin of coordinates is placed in the plane of the liquid–gas interface above the middle of the slot. The $x$-axis is defined along the pressure gradient, while the $y$-axis is aligned across the channel. According to Bazant & Vinogradova (2008) the general problem reduces to computing the two eigenvalues, $b_{eff}^{\parallel}$ and $b_{eff}^{\perp}$, which attain the maximal and minimal directional slip lengths, respectively.

The fluid flow satisfies Stokes equations

$$\eta\nabla^2\boldsymbol{u} = \nabla p, \quad \nabla\cdot\boldsymbol{u} = 0, \tag{2.1}$$

where $\boldsymbol{u}$ is the velocity vector, and the applied pressure gradient is parallel to the $x$-axis direction:

$$\nabla p_0 = (-\sigma, 0, 0). \tag{2.2}$$

The slip boundary conditions at the channel walls are defined in the usual way:

$$\boldsymbol{u}(x, 0, z) = b(x, z) \cdot \frac{\partial \boldsymbol{u}}{\partial y}(x, 0, z), \quad \hat{\boldsymbol{y}} \cdot \boldsymbol{u}(x, 0, z) = 0, \tag{2.3}$$

$$\boldsymbol{u}(x, H, z) = -b_H \cdot \frac{\partial \boldsymbol{u}}{\partial y}(x, H, z), \quad \hat{\boldsymbol{y}} \cdot \boldsymbol{u}(x, H, z) = 0. \tag{2.4}$$

Here the local slip length $b(x, z)$ is generally the function of both $x$ and $z$ coordinates. For simplicity, we now consider here the case $b_H = 0$. As the problem is linear in $\boldsymbol{u}$, we seek the solution in the form

$$\boldsymbol{u} = \boldsymbol{u}_0 + \boldsymbol{u}_1, \tag{2.5}$$

where $\boldsymbol{u}_0$ is the velocity of the flow over the homogeneous plane with the no-slip condition:

$$\boldsymbol{u}_0 = (u_0, 0, 0), \quad u_0 = -\frac{\sigma}{2\eta} y^2 + C_0^* y, \tag{2.6}$$

$$C_0^* \equiv \frac{\partial u_0}{\partial y}(y = 0) = \frac{\sigma H}{2\eta}, \tag{2.7}$$

and $\boldsymbol{u}_1$ is the perturbation of the flow, which is caused by the presence of the texture and decays far from the bottom of the channel.

We are interested in the effective slip length $\boldsymbol{b}_{eff}$ of the lower surface, which is defined as

$$b_{eff} = \frac{\langle u_s \rangle}{\left\langle \left( \dfrac{\partial u}{\partial y} \right)_s \right\rangle}, \tag{2.8}$$

where '$\langle \cdot \rangle$' means the average value in plane $xOz$.

### 2.1. *Longitudinal stripes*

In this case the problem is homogeneous in $x$ direction ($\partial/\partial x = 0$). The slip length $b(x, z) = b(z)$ is periodic in $z$ with period $L$. The elementary cell is determined as $b(z) = b$ at $|z| \leqslant \delta/2$, and $b(z) = 0$ at $\delta/2 < |z| \leqslant L$. In this case velocity $\boldsymbol{u}_1 = (u_1, 0, 0)$ has only one non-zero component, which can be determined by solving the Laplace equation with the boundary conditions discussed above. By choosing $L/(2\pi)$ as the length scale and $\sigma L^2/(4\pi^2\eta)$ as the velocity scale we obtain the following in the dimensionless form:

$$u_1(y, z) = \frac{a_0}{2} + \sum_{n=1}^{\infty} a_n \cos(nz) \mathrm{e}^{-ny}. \tag{2.9}$$

(The sine terms vanish due to symmetry.) Condition (2.3) leads to the dual trigonometric series

$$\frac{a_0}{2} + \sum_{n=1}^{\infty} a_n \left( 1 + \frac{2\pi b}{L} n \right) \cos(nz) = \frac{2\pi b}{L} C_0, \quad 0 < z \leqslant c, \tag{2.10}$$

$$\frac{a_0}{2} + \sum_{n=1}^{\infty} a_n \cos(nz) = 0, \quad c < z \leqslant \pi, \tag{2.11}$$

where $c = \pi\phi_2$ and $C_0 = C_0^* \cdot 2\pi\eta/(\sigma L) = \pi H/L$. To solve these series we assume that

$$\frac{a_0}{2} + \sum_{n=1}^{\infty} a_n \cos(nz) = \cos(z/2) \int_z^c \frac{h(t)\,\mathrm{d}t}{\sqrt{\cos z - \cos t}}, \quad 0 < z \leqslant c. \tag{2.12}$$

According to Sneddon (1966), we then get

$$a_0 = \frac{2}{\pi}\left[\frac{\pi}{\sqrt{2}} \int_0^c h(t)\,\mathrm{d}t\right], \tag{2.13}$$

$$a_n = \frac{2}{\pi}\left[\frac{\pi}{\sqrt{2}} \int_0^c h(t)\,(P_n(\cos t) + P_{n-1}(\cos t))\,\mathrm{d}t\right], \quad n = 1, 2, 3, \ldots, \tag{2.14}$$

where $P_n$ is the Legendre polynomial, and one can then show that the effective slip length is given by

$$b_{eff}^{\parallel} = \frac{L}{2\pi}\frac{a_0}{2C_0}. \tag{2.15}$$

By integrating (2.10) in the interval $[0, z]$, and substituting (2.12) and (2.14) we obtain $(0 < z \leqslant c)$

$$\frac{2\pi b}{L} \int_0^z \frac{h(t)\,\mathrm{d}t}{\sqrt{\cos t - \cos z}} = \sec\frac{z}{2}\left[\frac{2\pi b}{L} C_0 z - \int_0^z \cos\left(\frac{\xi}{2}\right) \int_\xi^c \frac{h(t)\,\mathrm{d}t}{\sqrt{\cos\xi - \cos t}}\,\mathrm{d}\xi\right]. \tag{2.16}$$

We further change the order of integration in brackets to get

$$\int_0^z \cos\left(\frac{\xi}{2}\right) \int_\xi^c \frac{h(t)\,\mathrm{d}t}{\sqrt{\cos\xi - \cos t}}\,\mathrm{d}\xi = \int_0^z h(t) \int_0^t \frac{\cos\left(\frac{\xi}{2}\right)\mathrm{d}\xi}{\sqrt{\cos\xi - \cos t}}\,\mathrm{d}t + \int_z^c h(t) \int_0^z \frac{\cos\left(\frac{\xi}{2}\right)\mathrm{d}\xi}{\sqrt{\cos\xi - \cos t}}\mathrm{d}t. \tag{2.17}$$

The evaluation of (2.16) gives

$$\int_0^z \frac{\cos\left(\frac{\xi}{2}\right)\mathrm{d}\xi}{\sqrt{\cos\xi - \cos t}} = \sqrt{2} \cdot \arcsin\left(\frac{\sin\frac{z}{2}}{\sin\frac{t}{2}}\right), \tag{2.18}$$

so that we get

$$\frac{2\pi b}{L} \int_0^z \frac{h(t)\mathrm{d}t}{\sqrt{\cos t - \cos z}} = \sec\frac{z}{2}\left[\frac{2\pi b}{L} C_0 z - \frac{\pi a_0}{2} + \sqrt{2}\int_z^c h(t) \arccos\left(\frac{\sin\frac{z}{2}}{\sin\frac{t}{2}}\right)\mathrm{d}t\right]. \tag{2.19}$$

This can be simplified by neglecting the last term in parentheses, which is small as compared to the main term $\pi a_0/2$ (due to properties of $\arccos(\sin(z/2)/\sin(t/2))$ and, thus,

$$h(t) = \frac{2}{\pi}\frac{\mathrm{d}}{\mathrm{d}t} \int_0^t \frac{\sin\frac{\xi}{2}}{\sqrt{\cos\xi - \cos t}} \left(C_0\xi - \frac{a_0\pi}{2 \cdot \frac{2\pi b}{L}}\right)\mathrm{d}\xi, \tag{2.20}$$

whence

$$a_0 = \frac{2\sqrt{2}}{\pi}\left[C_0 \cdot \pi\sqrt{2}\ln\left(\sec\frac{c}{2}\right) - \frac{a_0\pi}{2\cdot\dfrac{2\pi b}{L}}\cdot\sqrt{2}\ln\left(\sec\frac{c}{2}+\tan\frac{c}{2}\right)\right]. \tag{2.21}$$

In what follows,

$$b_{eff}^{\parallel} = \frac{L}{\pi}\frac{\ln\left[\sec\left(\dfrac{\pi\phi_2}{2}\right)\right]}{1+\dfrac{L}{\pi b}\ln\left[\sec\left(\dfrac{\pi\phi_2}{2}\right)+\tan\left(\dfrac{\pi\phi_2}{2}\right)\right]}. \tag{2.22}$$

### 2.2. *Transverse stripes*

In this case the pressure gradient depends on $x$, so that it is convenient to introduce a stream function $\psi(x, y)$ and the vorticity vector $\boldsymbol{\omega}(x, y)$. The two-dimensional velocity field corresponding to the transverse configuration is represented by $\boldsymbol{u}(x, y) = (\partial\psi/\partial y, -\partial\psi/\partial x, 0)$, and the vorticity vector $\boldsymbol{\omega}(x, y) = \nabla \times \boldsymbol{u} = (0, 0, \omega)$ has only one non-zero component, which is equal to

$$\omega = -\nabla^2\psi. \tag{2.23}$$

The solution can then be presented as the sum of the base flow with homogeneous no-slip condition and its perturbation due to the presence of stripes

$$\psi = \Psi_0 + \psi_1, \quad \omega = \Omega_0 + \omega_1, \tag{2.24}$$

where $\Psi_0$ and $\Omega_0$ correspond to a typical Poiseuille flow:

$$\Psi_0 = -\frac{\sigma}{\eta}\frac{y^3}{6} + C_0^*\frac{y^2}{2}, \quad \Omega_0 = \frac{\sigma}{\eta}y - C_0^*. \tag{2.25}$$

The problem for perturbations $\psi_1$ and $\omega_1$ of the stream function and $z$-component of the vorticity vector reads

$$\nabla^2\psi_1 = -\omega_1, \quad \nabla^2\omega_1 = 0, \tag{2.26}$$

which can be solved by applying boundary conditions (2.3) and (2.4) that take the following form: (Priezjev *et al.* 2005):

$$\frac{\partial\psi_1}{\partial y}(x, y=0) = b(x)\cdot\left[C_0^* - \omega_1(x, y=0)\right], \tag{2.27}$$

$$\frac{\partial\psi_1}{\partial y}(x, y=H) = 0, \tag{2.28}$$

and an extra condition that reflects our definition of the stream function

$$\psi_1(x, y=0) = 0. \tag{2.29}$$

This can be solved exactly to get

$$\omega_1(x, y) = \frac{\alpha_0}{2} + \sum_{n=1}^{\infty}\alpha_n\cos(\lambda_n x)\mathrm{e}^{-\lambda_n y}, \tag{2.30}$$

$$\psi_1(x, y) = -\frac{\alpha_0}{4}y^2 + \beta_0 y + \sum_{n=1}^{\infty}\left(\beta_n + \frac{\alpha_n}{2}\frac{y}{\lambda_n}\right)\cos(\lambda_n x)\mathrm{e}^{-\lambda_n y}, \tag{2.31}$$

where $\lambda_n = (2\pi n)/L$ is the wavenumber. Condition (2.28) leads to $\beta_0 = \alpha_0 H/2$, and (2.29) gives $\beta_n = 0$.

Applying boundary conditions, we obtain another dual series, which is similar to (2.10) and (2.11):

$$a_0\left(1+\frac{b}{H}\right)+\sum_{n=1}^{\infty}a_n\left(1+2\cdot\frac{2\pi b}{L}n\right)\cos(nx)=\frac{2\pi b}{L}C_0,\quad 0<x\leqslant c, \tag{2.32}$$

$$a_0+\sum_{n=1}^{\infty}a_n\cos(nx)=0,\quad c<x\leqslant\pi. \tag{2.33}$$

Here

$$a_0=\frac{4\pi^2\eta}{\sigma L^2}\beta_0,\quad a_n=\frac{\alpha_n}{2n}\frac{2\pi\eta}{\sigma L}, \tag{2.34}$$

and $b_{eff}^{\perp} = (L/2\pi)(a_0/C_0)$. Since $b/H$ is negligibly small, the dual series can be simplified to obtain

$$b_{eff}^{\perp}=\frac{L}{2\pi}\frac{\ln\left[\sec\left(\dfrac{\pi\phi_2}{2}\right)\right]}{1+\dfrac{L}{2\pi b}\ln\left[\sec\left(\dfrac{\pi\phi_2}{2}\right)+\tan\left(\dfrac{\pi\phi_2}{2}\right)\right]}. \tag{2.35}$$

### 2.3. *Arbitrary direction*

Here we consider the situation where the pressure gradient is aligned at the angle $\theta$ to the stripes. The surface velocity $\boldsymbol{u}_s = (u_s, 0, w_s)$ has only two non-zero components. We establish the coordinate system so that $-\nabla p_0$ is parallel to the $x$-axis. According to Bazant & Vinogradova (2008),

$$\langle \boldsymbol{u}_s\rangle = \boldsymbol{b}_{eff}\cdot\left\langle\left(\frac{\partial \boldsymbol{u}}{\partial y}\right)_s\right\rangle, \tag{2.36}$$

where $\boldsymbol{b}_{eff}$ is given by (1.2). Average components of surface velocity then read

$$\langle u_s\rangle = \left(b_{eff}^{\parallel}\cos^2\theta + b_{eff}^{\perp}\sin^2\theta\right)\cdot C_0^*, \tag{2.37}$$

$$\langle w_s\rangle = \left(b_{eff}^{\parallel} - b_{eff}^{\perp}\right)\sin\theta\cos\theta\cdot C_0^*. \tag{2.38}$$

The absolute value of the slip velocity on the striped SH surface $|\boldsymbol{U}_s|$ and the angle $\varphi$ between the driving force $(-\nabla p_0)$ and $\boldsymbol{U}_s$ are then given by

$$|\boldsymbol{U}_s| = \frac{\sigma H}{2\eta}\sqrt{(b_{eff}^{\parallel}\cos\theta)^2 + \left(b_{eff}^{\perp}\sin\theta\right)^2},\quad \tan\varphi = \frac{\left(b_{eff}^{\parallel} - b_{eff}^{\perp}\right)\sin\theta\cos\theta}{\left(b_{eff}^{\parallel}\cos^2\theta + b_{eff}^{\perp}\sin^2\theta\right)}. \tag{2.39}$$

## 3. Discussion

Figure 2(*a*) shows the theoretical eigenvalues of the slip-length tensor $\boldsymbol{b}_{eff}$ for slipping area fraction $\phi_2 = 0.5$ as a function of the slip length $b$ calculated using (2.22) and (2.35). In addition, we plot the data for tilted stripes ($\theta = \pi/4$). Also included in figure 2(*a*) are results of a numerical solution of the Stokes equations performed by C. Cottin-Bizonne and C. Barentin using the method developed in Cottin-Bizonne *et al.* (2004). The agreement between the theoretical and simulation data is very good for

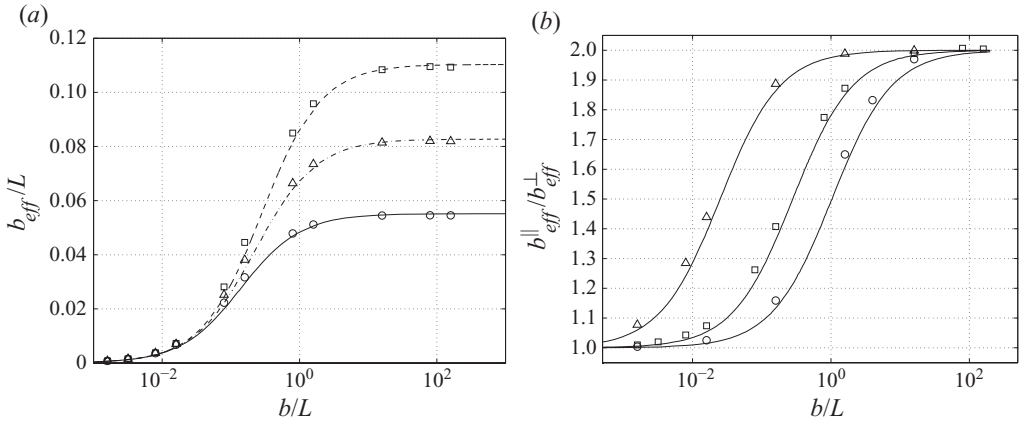


FIGURE 2. (*a*) Eigenvalues $b^{\parallel}_{eff}$ (dashed curve) and $b^{\perp}_{eff}$ (solid curve) of the slip-length tensor $\boldsymbol{b}_{eff}$ for stick-slip stripes of period $L$ and slipping area fraction $\phi_2 = 0.5$ as a function of the local slip length $b$ of this area. The dashed–dotted curve represents the effective slip in the direction of driving force for tilted ($\theta = \pi/4$) stripes. Symbols show numerical results. (*b*) The ratio of theoretically predicted eigenvalues of the slip-length tensor $b_{eff}$ (solid curves) and corresponding results of numerical modelling (symbols). From left to right, $\phi_2 = 0.05,\ 0.5$ and 0.95.

all $\phi_2$ and $b/L$, but at $b/L = O(1)$ there is some small discrepancy, suggesting that our formulas slightly underestimate the effective slip, which is likely due to a simplification of (2.19). The same trends were observed for other values of $\phi_2$. Still, our analytical expressions for the effective slip, (2.22) and (2.35), appear to be surprisingly accurate, especially taking into account their simplicity. The same remark concerns the use of tensorial formula (1.2).

Our results imply that the flow past stripes is controlled by the ratio of the local slip length $b$ to texture period $L$. At $b/L \gg 1$ our expressions for $b_{eff}$ turn to (1.1), suggested earlier for a perfect local slip. As expected, the effective slip decreases when $b/L = O(1)$ and smaller. Interestingly, this ratio also controls the anisotropy of the flow. Indeed, combining (2.22) and (2.35) we get

$$b^{\parallel}_{eff} = b^{\perp}_{eff}\left(1 + \frac{1}{1 + \dfrac{L}{\pi b}\ln\left[\sec\left(\dfrac{\pi\phi_2}{2}\right) + \tan\left(\dfrac{\pi\phi_2}{2}\right)\right]}\right). \tag{3.1}$$

If $b/L \gg 1$, the effective slip for parallel stripes, $b^{\parallel}_{eff}$, is twice that of perpendicular stripes, $b^{\perp}_{eff}$, as it was in the case of a perfect slip ($b_2 = \infty$) at the liqud–gas interface (Lauga & Stone 2003; Cottin-Bizonne *et al.* 2004; Sbragaglia & Prosperetti 2007; Bahga, Vinogradova & Bazant, 2010). In this case surface anisotropy leads to a truly tensorial effective slip. However, anisotropy of the flow decreases with a decrease in $b/L$, and at small $b/L$ we get $b^{\parallel,\perp}_{eff} \sim b$. In other words, at small local slip we predict simple surface-averaged isotropic flows (independent of orientation), which means despite the fact that the local slip varies in only one direction, the effective slip is scalar. These unexpected results are summarized in figure 2(*b*). This finding can be understood by using the following simple arguments. Following the advice of H. A. Stone (2009 private communication), let us consider the average fluid velocity

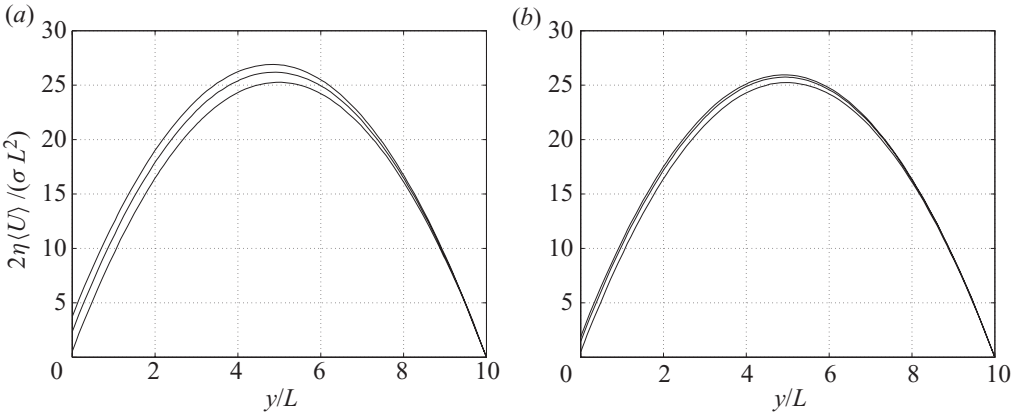


FIGURE 3. Average velocity profiles ($\phi_2 = 0.8$) for a longitudinal ($a$) and transverse ($b$) flow. From top to bottom $b/L = 1000$, 1 and 0.1.

$\langle u_s \rangle$ on the SH surface. According to boundary condition (2.3),

$$\langle u_s \rangle = \frac{1}{L^2}\int_0^L \int_0^L u_s(x,z)\,\mathrm{d}x\,\mathrm{d}z = \frac{1}{L^2}\int_0^L \int_0^L b(x,z)\left(\frac{\partial u}{\partial y}\right)_s \mathrm{d}x\,\mathrm{d}z. \tag{3.2}$$

For transverse flow this expression takes the form

$$\langle u_s \rangle = \frac{1}{L}\int_0^\delta b\left[C_0^* + \left(\frac{\partial u_1}{\partial y}\right)_s\right]\mathrm{d}x = bC_0^*\phi_2 + \frac{b}{L}\int_0^\delta \left(\frac{\partial u_1}{\partial y}\right)_s \mathrm{d}x, \tag{3.3}$$

where $C_0^* = (\partial u_0/\partial y)_s = \text{constant}$ is, obviously, independent of the relative orientation of stripes with respect to a pressure gradient, since $u_0$ represents the solution of the problem for a smooth homogeneous surface. The same arguments apply in the longitudinal case, where the only difference would be the integration over $z$ instead of $x$. Therefore, when $b$ is a small value ($b/L = O(\varepsilon)$), the second term in (3.3) may be neglected as an infinitely small value of higher (second) order because $u_1 \propto \varepsilon$, and, thus,

$$\left(\boldsymbol{b}_{eff}\right)_{b\to 0} \approx b\phi_2 + O\left(\varepsilon^2\right) \tag{3.4}$$

is independent of an external force direction. The anisotropy of the effective slip is determined by the second integral term in (3.3), which dominates when $b/L = O(1)$ and larger. These results suggest that both the value (upper limit) of the effective slip length and the anisotropy of the flow are controlled by the smallest characteristic length of the problem (in our case, $b$ or $\delta$).

Finally, we present average velocity profiles in longitudinal ($\theta = 0$) and transverse ($\theta = \pi/2$) configurations for different values of the local slip length $b$ (figure 3). Mean flow remains two-dimensional and parabolic when the driving force is applied in main directions, yet both the average slip velocity at $y = 0$ and the maximal velocity value at the middle of the channel depend on $b$. For arbitrary $\theta$ the flow is essentially three-dimensional as the orthogonal velocity component appears due to the tensorial effective boundary condition (2.36).

## 4. Conclusion

We have analysed a pressure-driven flow over striped SH surfaces. Unlike the previous approach, we have obtained general analytical solutions for any value of

local partial slip. We have confirmed that the hydrodynamic response of a striped slipping surface is generally anisotropic. Our main conclusion is that both effective slip and flow anisotropy are controlled by the ratio of local slip at the gas area to texture size. When this ratio is large, our results are closely related to those of Lauga & Stone (2003), Cottin-Bizonne *et al.* (2004), Sbragaglia & Prosperetti (2007) and Bahga *et al.* (2010), and surface anisotropy leads to anisotropy of effective slip. For a small ratio we predict not only a decrease in the effective slip, but also a different isotropic response of the striped SH surface.

The advice of H. A. Stone is gratefully acknowledged. We thank C. Cottin-Bizonne and C. Barentin for numerical verification of the theory. This research was supported by the DFG under the Priority programme 'Micro and nanofluidics' (grant Vi 243/1-3) and by the RAS under the Priority Programme 'Assembly and Investigation of Macromolecular Structures of New Generations'.

## REFERENCES

Bahga, S. S., Vinogradova, O. I. & Bazant, M. Z. 2010 Anisotropic electro-osmotic flow over super-hydrophobic surfaces. *J. Fluid Mech.* **644**, 245–255.

Bazant, M. Z. & Vinogradova, O. I. 2008 Tensorial hydrodynamic slip. *J. Fluid Mech.* **613**, 125–134.

Bocquet, L. & Barrat, J. L. 2007 Flow boundary conditions from nano- to micro-scales. *Soft Matter* **3**, 685–693.

Choi, C. H., Ulmanella, U., Kim, J., Ho, C. M. & Kim, C. J. 2006 Effective slip and friction reduction in nanograted superhydrophobic microchannels. *Phys. Fluids* **18**, 087105.

Cottin-Bizonne, C., Barentin, C., Charlaix, E., Bocquet, L. & Barrat, J. L. 2004 Dynamics of simple liquids at heterogeneous surfaces: molecular-dynamic simulations and hydrodynamic description. *Eur. Phys. J.* E **15**, 427–438.

Cottin-Bizonne, C., Barrat, J. L., Bocquet, L. & Charlaix, E. 2003 Low-friction flows of liquid at nanopatterned interfaces. *Nat. Mater.* **2**, 237–240.

Cottin-Bizonne, C., Cross, B., Steinberger, A. & Charlaix, E. 2005 Boundary slip on smooth hydrophobic surfaces: intrinsic effects and possible artifacts. *Phys. Rev. Lett.* **94**, 056102.

Davis, A. M. J. & Lauga, E. 2009 Geometric transition in friction for flow over a bubble mattress. *Phys. Fluids* **21**, 011701.

Feuillebois, F., Bazant, M. Z. & Vinogradova, O. I. 2009 Effective slip over superhydrophobic surfaces in thin channels. *Phys. Rev. Lett.* **102**, 026001.

Hyväluoma, J. & Harting, J. 2008 Slip flow over structured surfaces with entrapped microbubbles. *Phys. Rev. Lett.* **100**, 246001.

Joly, L., Ybert, C. & Bocquet, L. 2006 Probing the nanohydrodynamics at liquid–solid interfaces using thermal motion. *Phys. Rev. Lett.* **96**, 046101.

Joseph, P., Cottin-Bizonne, C., Benoît, J. M., Ybert, C., Journet, C., Tabeling, P. & Bocquet, L. 2006 Slippage of water past superhydrophobic carbon nanotube forests in microchannels. *Phys. Rev. Lett.* **97**, 156104.

Lauga, E., Brenner, M. P. & Stone, H. A. 2007 *Handbook of Experimental Fluid Dynamics*, Ch. 19, pp. 1219–1240. Springer.

Lauga, E. & Stone, H. A. 2003 Effective slip in pressure-driven stokes flow. *J. Fluid Mech.* **489**, 55–77.

Ou, J., Moss, J. M. & Rothstein, J. P. 2007 Enhanced mixing in laminar flows using ultrahydrophobic surfaces. *Phys. Rev.* E **76**, 016304.

Ou, J. & Rothstein, J. P. 2005 Direct velocity measurements of the flow past drag-reducing ultrahydrophobic surfaces. *Phys. Fluids* **17**, 103606.

Philip, J. R. 1972 Flows satisfying mixed no-slip and no-shear conditions. *J. Appl. Math. Phys.* **23**, 353–372.

Priezjev, N. V., Darhuber, A. A. & Troian, S. M. 2005 Slip behaviour in liquid films on surfaces of patterned wettability. *Phys. Rev.* E **71**, 041608.

Quere, D. 2005 Non-sticking drops. *Rep. Prog. Phys.* **68**, 2495–2532.

Sbragaglia, M. & Prosperetti, A. 2007 A note on the effective slip properties for microchannel flows with ultrahydrophobic surfaces. *Phys. Fluids* **19**, 043603.

Sneddon, I. N. 1966 *Mixed Boundary Value Problems in Potential Theory*. North-Holland.

Squires, T. M. & Quake, S. R. 2005 Microfluidics: fluid physics at the nanoliter scale. *Rev. Mod. Phys.* **77**, 977–1026.

Stone, H. A., Stroock, A. D. & Ajdari, A. 2004 Engineering flows in small devices. *Annu. Rev. Fluid Mech.* **36**, 381–411.

Vinogradova, O. I. 1995 Drainage of a thin liquid film confined between hydrophobic surfaces. *Langmuir* **11**, 2213–2220.

Vinogradova, O. I. 1999 Slippage of water over hydrophobic surfaces. *Intl J. Miner. Process.* **56**, 31–60.

Vinogradova, O. I., Bunkin, N. F., Churaev, N. V., Kiseleva, O. A., Lobeyev, A. V. & Ninham, B. W. 1995 Submicrocavity structure of water between hydrophobic and hydrophilic walls as revealed by optical cavitation. *J. Colloid Interface Sci.* **173**, 443–447.

Vinogradova, O. I., Koynov, K., Best, A. & Feuillebois, F. 2009 Direct measurements of hydrophobic slipage using double-focus fluorescence cross-correlation. *Phys. Rev. Lett.* **102**, 118302.

Vinogradova, O. I. & Yakubov, G. E. 2003 Dynamic effects on force measurements. II. Lubrication and the atomic force microscope. *Langmuir* **19**, 1227–1234.

Ybert, C., Barentin, C., Cottin-Bizonne, C., Joseph, P. & Bocquet, L. 2007 Achieving large slip with superhydrophobic surfaces: scaling laws for generic geometries. *Phys. Fluids* **19**, 123601.